Science of Sintering, **55** (2023) 11-27

https://doi.org/10.2298/SOS2301011T

UDK: 621.742.48; 622.785

Application of Artificial Neural Networks in Performance Prediction of Cement Mortars with Various Mineral Additives

Anja Terzić[1*)], Milada Pezo[2], Lato Pezo[3]
[1]Institute for Materials Testing - IMS, Vojvode Mišića Bl. 43, 11000 Belgrade, Serbia
[2]Department of Thermal Engineering and Energy, "Vinča" Institute of Nuclear Sciences -National Institute of the Republic of Serbia, University of Belgrade, P.O. Box 522, 11001 Belgrade, Serbia
[3]Institute of General and Physical Chemistry, University of Belgrade, Studentski Trg 12-16, 11000 Belgrade, Serbia

Abstract:
The machine learning technique for prediction and optimization of building material performances became an essential feature in the contemporary civil engineering. The Artificial Neural Network (ANN) prognosis of mortar behavior was conducted in this study. The model appraised the design and characteristics of seventeen either building or high-temperature mortars. Seven different cement types were employed. Seventeen mineral additives of primary and secondary origin were embedded in the mortar mixtures. Cluster Analysis and Principal Component Analysis designated groups of similar mortars assigning them a specific purpose based on monitored characteristics. ANN foresaw the quality of designed mortars. The impact of implemented raw materials on the mortar quality was assessed and evaluated. ANN outputs highlighted the high suitability level of anticipation, i.e., 0.999 during the training period, which is regarded appropriate enough to correctly predict the observed outputs in a wide range of processing parameters. Due to the high predictive accuracy, ANN can replace or be used in combination with standard destructive tests thereby saving the construction industry time, resources, and capital. Good performances of altered cement mortars are positive sign for widening of economical mineral additives application in building materials and making progress towards achieved carbon neutrality by reducing its emission.
Keywords*: Masonry Cements; High-temperature Cements; Industrial byproducts; Low-cost primary raw materials; Circular economy.*

1. Introduction

There is a constant tendency regarding widening of low-cost mineral additives application in the building materials sector in order to make progress towards reduction of carbon emission and to achieve carbon neutrality in indoor and outdoor spaces. Therefore, natural pozzolana and industrial byproducts are often employed as supplementary admixtures in cement-based materials such as concrete and mortar. These additives not only replace cement thereby influencing the reduction of CO_2 emission in the atmosphere, they also play

[*)] **Corresponding author:** anja.terzic@institutims.rs

an important role in the modification of cementitious material microstructure, they rearrange chemical reactions routes within cement, and finally they incite changes in mechanical and thermal properties of building materials [1-6].

Various mineral additives have been employed in the design of mortar and concrete over past few decades. Each of these either primary or secondary raw materials has positive as well as negative effects on the performances of the construction materials. The chemical composition of a mineral additive strongly influences and modifies chemical reactions that define hydration and subsequent solidification of the observed building material. Besides its chemical composition, physical and morphological characteristics of mineral additive particles (specific surface area, grain size, diameter and shape) impact properties and final behavior of the material. Probably the most effective admixtures to modify the microstructure of a cementitious material are nano silica, micro silica and silica fume [7-10]. The silica based mineral additives bestow cement mortar and concrete properties (compressive strength, flexural strength) due to their pozzolanic reaction and smaller particle sizes than cement particles. Limestone powder, fly ash and bottom ash (coal combustion byproducts), and zeolite are frequently employed pozzolana resources in the new paradigm of the circular economy [11-17]. Limestone powder is frequently utilized for achieving a target flow of fresh mixture. This additive induces high early dimensional stability [12]. Fly ash reduces early heat of hydration and decreases volume stability issues in different exposure conditions. Fly ash requires higher water demands than cement, but it provides denser microstructure [15]. Zeolite performances are between those of limestone and fly ash. The addition of natural zeolite leads to an improvement in mechanical strengths, durability properties, and weather resistance of cementitious material [16]. Due to bentonite outstanding water swelling properties, it is used in mortar or concrete to fill the small voids in order to decrease the water migration withing the pore structure. This enables excellent waterproofing and impermeability characteristics of the building composite. Bentonite does not have significant influence on the compressive strength; however, it influences notable improvement in sulfate attack resistance [17-22]. Similar to zeolite, the addition of bentonite to the cement matrix effectively reduces the leaching rate of the radionuclides and heavy metals [16, 20]. Copper slag employed as a replacement for cementing binder or as an admixture has considerable influence on the mechanical properties, durability, as well as thermo-mechanical behavior [23]. Clay, usually activated by acids or by thermal or alkaline methods, as well as kaolin or chamotte grog is widely used low cost pozzolanic materials [24-26]. Powdery alumina incorporation leads to long-term improvements in strength of cementitious material due to the increase in monosulfate content. Namely, the formation of additional monosulfate phases increases solid volume, reduces porosity, and refines pore structure in the cement paste, consequently leading to an enhancement of strength at later ages [27]. Perlite, vermiculite, spinel, and pyrophyllite are often employed to augment the thermal characteristic such as compressive strength after firing [28-31].

Artificial intelligence methods such as artificial neural networks (ANNs) are becoming more in demand as they are extensively used by many researchers in a variety of engineering applications [32-34]. In recent years, studies were reported in which the ANN are employed to estimate the various mechanical properties of cementitious building materials (mortar of concrete) containing different types of mineral additives [35-38]. Usually compressive strengths (CS), as the most important parameter of mortar’s quality, are predicted by application of two different multilayer ANN architectures on a large number different mixtures (each one comprising number of specimens pinpointed in adequate EN standard for CS testing) [37]. As a result, the tested characteristic of mortar containing specific mineral additive can be predicted in the multilayer feed forward ANN model. Despite the ongoing extensive research in this field, there is still no universal model for the prediction of simultaneous effects of additives on mortar properties which would minimize the experimental work as well as save cost and time.

The aim of the proposed ANN model in this study is to assess the influence of the chemical composition of seventeen mineral additives (fly ash, bottom ash, zeolite, bentonite, perlite, vermiculite, pyrophyllite, micro silica, silica fume, spinel, chamotte grog, calcinated clay, kaolin clay, alumina, limestone, talc, and copper slag) on the quality of cement mortars indicated using following parameters: heat of hydration (HH), setting time (IST, FST), cold compressive strength (CCS), cold flexural strength (CFS), hot compressive strength (HCS), refractoriness (SK, SK-T), and sulphate resistance (SR). The accomplishment of ANN is matched to experimental results. Normalized form of the input parameters is obtained and applied in the mentioned models in order to increase the correlation between input parameters and target to predict more accurate properties of cement mortars. The developed ANN model displays high predictive accuracy and can replace or be used in combination with standard destructive tests thereby saving the construction industry time, resources, and capital.

2. Materials and Experimental Procedures

Seventeen experimental mortars were prepared for this study. The labels of mortar samples, abbreviations used for the employed raw materials, i.e. cements and mineral additives, as well as their mix-designs are provided in Table I. Initial six cement mortar samples (M-OPC, M-MHHC, M-HESC, M-LHHC, M-HSCR, M-CAC, and M-HAC) were used as reference samples in the analytical modeling i.e., for comparison and differentiation of altered mortars – mortars with mineral additives (M-FA, M-BA, M-Z, M-B, M-Pr, M-V, M-Py, M-MS, M-SF, M-Sp, M-CG, M-Cc, M-Kc, M-Ap, M-L, M-T, and M-CS).

The mortar samples were prepared according to the standard procedure provided in SRPS EN 480-1:2015. Mineral additives were employed in quantities from 10 to 20 % (calculated from the mass of cement), with respect to EN 197-1, as given in Table I. The aggregate comprised three fractions (-0.2+0.6; -0.6+1.0; and -1.0+2.0 mm) of either quartz or corundum sand in 1:1:1 ratio.

Pozzolanic activity (PA) was estimated for each mineral additive individually according to the procedure described in SRPS EN 196-5:2012. In order to maintain the simplicity of comparisons during analytical modeling it was adopted that cements (OPC, MHHC, HESC, LHHC, HSCR, CAC, and HAC) exhibit the highest pozzolanic activity (marked with number 5). Compressive strength of each altered mortar is lower than that of standard cement mortar. Therefore, depending on the obtained compressive strength value, each of mineral additives was correlated to a mark ranging from 4 to 1 (higher mark indicates higher strength i.e., higher PA).

The hydration heath (HH) was obtained by isothermal conduction calorimetry method described in SRPS EN 196-11:2019. Setting times (IST and FST) were determined according to SRPS EN 196-3:2019 (Determination of setting times and soundness). Compressive and flexural strengths were tested on 4×4×16 cm prismatic samples in accordance with SRPS EN 196-1:2017 (Detrmination of strength). Mechanical strenths were measured after 3, 7, 14, 21, and 28 days upon preparation of the samples. Hot compressive strength was obtained on the fired mortar samples. Upon 28 days old of curing and solidification, the prismatic samples (4×4×16 cm) were submitted to the thermal treatment in a laboratory furnace at following temperatures: 100, 500, 800, and 1000 °C. The rate of heating rate was 100 °C/h with 2 hours delay upon reaching the targeted temperature. Refractoriness (SK – number of equivalent pyrometric cone, and SK/T – melting temperature of equivalent pyrometric cone in °C) was estimated according to ASTM C24-09 (2018) - Standard test method for pyrometric cone equivalent (PCE) of fireclay and high-alumina refractory materials. Sulphate resistance was tested according to the SRPS CEN/TR 15697:2014 Cement - Performance testing for sulfate resistance - State of the art report. In order to simplify analytical modeling SR of the cement mortars and altered mortars was indicated by marks ranging from 1 to 3, i.e., “low – moderate – excellent” system where higher mark reveals better sulphate resistance of tested material.

Cluster analysis (CA) was undertaken to categorize and discriminate mortar samples i.e., cement mortars (M-OPC, M-MHHC, M-HESC, M-LHHC, M-HSCR, M-CAC, and M-HAC) and altered mortars (M-FA, M-BA, M-Z, M-B, M-Pr, M-V, M-Py, M-MS, M-SF, M-Sp, M-CG, M-Cc, M-Kc, M-Ap, M-L, M-T, and M-CS). All samples were aggregated in a twenty-four-dimensional space. Complete linkage was used for analytical modeling. City-block (Manhattan) distance was evaluated in cluster analysis.

Tab. I Mix designs of experimental mortars.

Mortar	Cement (type), %	Mineral additive, %	Aggregate, %	
			Quartz	Corundum
M-OPC	25 (OPC)	-	75	-
M-MHHC	25 (MHHC)	-	75	-
M-HESC	25 (HESC)	-	75	-
M-LHHC	25 (LHHC)	-	75	-
M-HSCR	25 (HSCR)	-	75	-
M-CAC	20 (CAC)	-	-	80
M-HAC	20 (CAC)	-	-	80
M-FA	20 (OPC)	5	75	-
M-BA	20 (OPC)	5	75	-
M-Z	21.25 (OPC)	3.75	75	-
M-B	21.25 (OPC)	3.75	75	-
M-Pr	21.25 (OPC)	3.75	75	-
M-V	21.25 (OPC)	3.75	75	-
M-Py	17.5 (OPC)	7.5	75	-
M-MS	22.5 (OPC)	2.5	75	-
M-SF	22.5 (OPC)	2.5	75	-
M-Sp	17 (CAC)	3	-	80
M-CG	17 (CAC)	3	-	80
M-Cc	21.25 (OPC)	3.75	75	-
M-Kc	17 (CAC)	3	-	80
M-Ap	17 (CAC)	3	-	80
M-L	20 (OPC)	5	75	-
M-T	17 (CAC)	3	-	80
M-CS	21.25 (OPC)	3.75	75	-

Cement: OPC - Ordinary Portland cement; MHHC - Moderate heat hydration cement; HESC - High early strength cement; LHHC - Low heat hydration cement; HSCR - High sulphate resistant cement; CAC - Calcium aluminate cement; HAC - High alumina cement;
Additive: FA - Fly ash; BA - Bottom ash; Z - Zeolite; B - Bentonite; Pr - Perlite; V - Vermiculite; Py - Pyrophyllite; MS - Micro silica; SF - Silica fume; Sp - Spinel (powder); CG - Chamotte grog; Cc - Clay (calcinated clay); Kc - Kaolin clay; Ap - Alumina (powder); L - Limestone; T - Talc; CS - Copper slag.

Tab. II Chemical compositions of experimental mortars.

Mortar	SiO_2, %	Al_2O_3, %	Fe_2O_3, %	CaO, %	MgO, %	K_2O, %	Na_2O, %	TiO_2, %	SO_3, %	LoI, %
M-OPC	76.42	2.02	0.99	15.85	0.72	0.36	0.05	0.015	0.567	0.725
M-MHHC	75.92	1.87	1.64	15.48	1.05	0.22	0.04	0.015	0.372	0.675
M-HESC	75.45	1.71	0.87	16.92	0.86	0.29	0.07	0.015	0.820	0.700
M-LHHC	76.80	1.66	1.27	15.58	0.82	0.16	0.06	0.015	0.547	0.740
M-HSCR	78.26	1.46	1.07	15.21	0.39	0.21	0.07	0.192	0.22	0.585
M-CAC	1.80	88.51	1.67	7.32	0.14	0.04	0.05	0.392	0.014	0.276
M-HAC	0.14	93.80	0.12	5.55	0.02	0.02	0.08	0.008	0.002	0.168
M-FA	78.43	2.63	1.19	13.03	0.70	0.36	0.06	0.017	0.496	0.807
M-BA	78.12	2.71	1.14	13.16	0.68	0.37	0.08	0.041	0.489	0.929
M-Z	77.98	2.24	0.93	13.589	0.63	0.35	0.07	0.015	0.481	1.165
M-B	77.72	2.36	0.98	13.51	0.73	0.36	0.23	0.027	0.478	1.063
M-Pr	78.32	2.31	0.91	13.54	0.62	0.51	0.16	0.017	0.482	0.852
M-V	5.80	76.48	1.54	13.10	1.83	0.27	0.03	0.06	0.316	0.193
M-Py	79.99	2.73	0.87	11.67	0.59	0.34	0.06	0.027	0.398	1.363
M-MS	78.29	1.89	0.94	14.30	0.65	0.34	0.04	0.015	0.515	0.721
M-SF	78.11	1.88	0.91	14.32	0.65	0.34	0.08	0.015	0.561	0.801
M-Sp	1.55	89.32	1.43	6.23	0.93	0.03	0.06	0.343	0.0119	0.259
M-CG	3.05	87.69	1.87	6.37	0.19	0.08	0.12	0.401	0.094	0.312
M-Cc	77.65	2.40	0.99	13.56	0.68	0.34	0.05	0.080	0.540	1.410
M-Kc	3.32	88.02	1.48	6.25	0.12	0.04	0.05	0.334	0.012	0.537
M-Ap	1.54	90.20	1.42	6.22	0.12	0.03	0.05	0.334	0.012	0.243
M-L	75.43	1.75	0.83	15.49	0.62	0.31	0.04	0.016	0.454	2.767
M-T	3.05	87.23	1.61	6.23	1.11	0.03	0.05	0.335	0.012	0.525
M-CS	76.25	2.07	2.97	13.72	0.77	0.36	0.07	0.015	0.4883	0.822

Principal Component Analysis (PCA) was used in exploratory data analysis. The procedure was performed by Eigenvalue decomposition of a data correlation matrix [39]. The first component has the largest possible variance. The maximum separation among clusters of parameters is acquired by this analysis. Considerable reduction in a number of variables and the detection of structure in the relationship between measuring parameters is achieved. The full auto scaled data matrix consisting of different mortar mixtures was submitted to the PCA, which resulted in spatial relationship between processing parameters (mortar properties) and formed graphic differentiation between observed samples.

The assessing of CA and PCA of the acquired results was executed using Statistica software version 12 (StatSoft Inc. 2013, USA)®.

Artificial Neural Network model (ANN) was used in the prediction of values of the experimental data i.e., tested properties (PA, HH, IST, FST, CCS-d, CFS-d, HCS-T, SK, and SR). The database for ANN was randomly divided into: training data (60 %), cross-validation (20 %), and testing data (20 %). The cross-validation data set was used to test the performance of the network, while training was in progress as an indicator of the level of generalization and the time at which the network has begun to over-train. The testing data set was used to examine the network generalization capability. To improve the ANN behavior, both input and output data were normalized. In order to obtain good network behavior, it is necessary to conduct a trial-and-error procedure and also to choose the number of hidden layers, and the number of neurons in hidden layer(s). In this analysis, a Multilayer Perceptron Model (MLP) comprised three layers (input, hidden and output). These architectures were used in parameters anticipation, and have been certified as entirely proficient of approximating nonlinear functions [40]. Broyden-Fletcher-Goldfarb-Shanno (BFGS) algorithm was engaged for solution of the unconstrained nonlinear optimization in the ANN modelling [41].

The weight coefficients and biases connected to the hidden and output layers of the ANN model are introduced in matrices and vectors W_1 and B_1, and W_2 and B_2, respectively. The neural network model can be outlined by matrix notation:

$$Y = f_1(W_2 \cdot f_2(W_1 \cdot X + B_1) + B_2) \quad (1)$$

where Y is the matrix of the outputs, f_1 and f_2 are transfer functions in the hidden and output layers, accordingly, and X is the matrix of inputs [42].

The optimum count of hidden neurons was selected upon minimizing the divergence among anticipated ANN values and desired outputs, using r^2 during testing as a performance indicator.

The Yoon's global sensitivity equation was used to calculate the relative impact of the input parameters on output variables, according to weight coefficients of the developed ANN models [43]:

$$RI_{ij}(\%) = \frac{\sum_{k=0}^{n}(w_{ik} \cdot w_{kj})}{\sum_{i=0}^{m}\left|\sum_{k=0}^{n}(w_{ik} \cdot w_{kj})\right|} \cdot 100\% \quad (2)$$

where: w - weight coefficient in ANN model, i - input variable, j - output variable, k - hidden neuron, n - number of hidden neurons, m - number of inputs.

The numerical verification of the developed models was tested using coefficient of determination (r^2), reduced chi-square (χ^2), mean bias error (*MBE*), root mean square error (*RMSE*) and mean percentage error (*MPE*). These commonly used parameters can be calculated as follows:

$$\chi^2 = \frac{\sum_{i=1}^{N}(x_{\exp,i} - x_{pre,i})^2}{N - n}, \; RMSE = \left[\frac{1}{N} \cdot \sum_{i=1}^{N}(x_{pre,i} - x_{\exp,i})^2\right]^{1/2},$$

$$MBE = \frac{1}{N} \cdot \sum_{i=1}^{N}(x_{pre,i} - x_{\exp,i}), \; MPE = \frac{100}{N} \cdot \sum_{i=1}^{N}\left(\frac{\left|x_{pre,i} - x_{\exp,i}\right|}{x_{\exp,i}}\right) \quad (3)$$

where $x_{exp,i}$ stands for the experimental values and $x_{pre,i}$ are the predicted values calculated by the model for these measurements. N and n are the number of observations and constants, respectively.

3. Results and Discussion

The following properties of the experimental mortar samples were monitored: pozzolanic activity for mineral additive (PA), heat of hydration (HH), J/g; initial setting time (IST), min; final setting time (FST), min; cold compressive strength after d = 3, 7, 14, 21, and 28 days (CCS-d), MPa; cold flexural strength after d = 3, 7, 14, 21, and 28 days (CFS-d), MPa; hot compressive strength after firing at T=100, 500, 800, and 1000ºC (HCS-T), MPa; refractoriness (SK and SK/T, °C); and sulphate resistance (SR), MPa. Experimentally obtained data are presented in Table III.

3.1. Correlation analysis

The correlation analysis was employed in investigation of the relations between output variables i.e., properties of experimental mortars. The obtained results are visualized and displayed in Figure 1. It can be noticed that the darker blue color of the squares, which shows the two variables relation, presents a stronger correlation between these variables. On the other hand, the lighter tone suggests a certain difference between two variables.

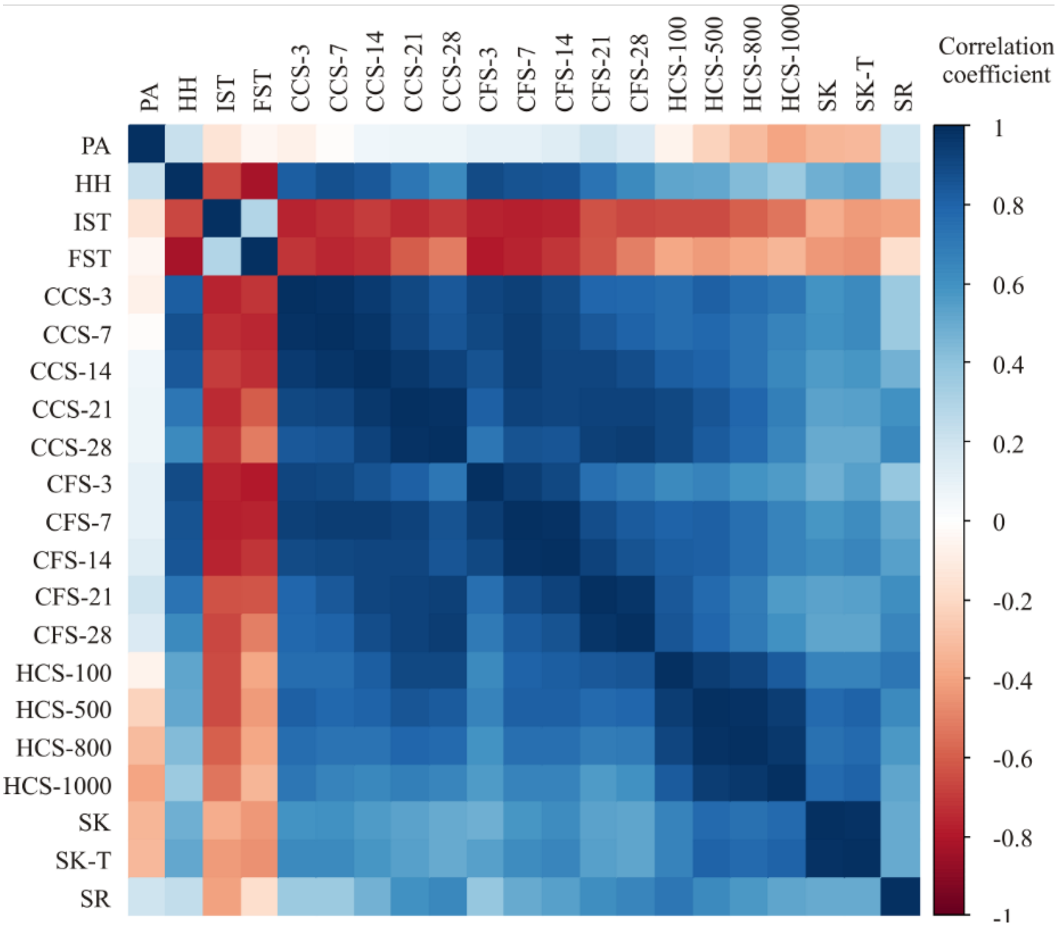

Fig. 1. Correlation analysis between output variables (mortar properties).

As seen in Fig. 1, the heat of hydration (HH) has strong influence over early mechanical strengths. Both compressive and flexural strengths of all investigated mortars, cement based- and altered mortar samples alike, are directly influenced by HH parameter. The strongest relation is visible for compressive and flexural strengths measured after three days (CCS-3 and CFS-3), and it decreases over time. Relations between HH and mechanical strengths developed from 7th to 14th day - CCS-7, CCS-14, CFS-7, and CFS-14, respectively, are marked as strong by exhibiting correlation coefficient value between 0.8 and 1. Initial and final setting times (IST, FST) are indirectly correlated to early compressive and flexural strengths (CCS-3, CCS-7, CFS-3, CFS-7) since their correlation coefficient ranges between -0.8 and -0.9. IST and FST parameters have slight influence over hot compressive strengths (HCS-100, HCS-500, HCS-800, and HCS-1000) as their correlation coefficients vary between -0.4 and -0.6. Cold compressive strengths are directly correlated to flexural strengths (correlation coefficients = 0.8-1), as well as with hot compressive strengths (correlation coefficients = 0.6-0.8). Refractoriness is directly dependent on hot compressive strengths (correlation coefficients = 0.7-0.9). Sulphate resistance is directly correlated to compressive and flexural strengths (correlation coefficients = 0.6-0.7).

Tab. III Experimentally obtained properties of cement mortars and altered mortars.

	PA	HH	IST	FST	CCS-3	CCS-7	CCS-14	CCS-21	CCS-28	CFS-3	CFS-7	CFS-14	CFS-21	CFS-28	HCS-100	HCS-500	HCS-800	HCS-1000	SK	SK-T	SR
M-OPC	5	320	165	225	31.25	41.15	47.2	49.05	50.3	6.8	7.5	8.7	9.4	9.5	48.4	27.9	20.1	21.5	9	1280	1
M-MHHC	5	275	180	255	22.7	31.9	48.1	53.6	65.1	5.2	5.7	6.4	12.4	14.3	40.5	25.3	15.4	15.5	8	1250	2
M-HESC	5	375	105	160	42.6	55.2	59.4	61.8	63.7	8.9	9.5	11.6	12.7	13.5	39.8	26.1	16.7	16.8	8	1250	1
M-LHHC	5	260	95	480	13.7	17.9	26.8	42.8	49.8	4.1	4.5	5.7	7.2	9.4	48.3	27.7	20.2	20.9	9	1280	2
M-HSCR	5	275	160	230	14.1	16.9	32.4	48.3	51.7	6.6	7.3	8.5	9.2	9.5	48.1	27.3	20	20.5	10	1300	3
M-CAC	5	370	90	155	53.8	67.8	75.2	81.3	84.1	9.3	11.8	14.2	15.9	16.2	81.1	71.2	63.1	45.3	20	1530	3
M-HAC	5	375	90	155	61.7	78.5	83.5	87.9	91.5	9.8	12.5	15.3	17.1	18.7	90.8	81.4	65.2	55.5	34	1750	3
M-FA	4	360	110	170	45.3	56.2	60.8	61.9	63.9	8.9	9.3	11.3	12.5	13.6	53.7	41.6	30.2	31.3	20	1530	2
M-BA	3	355	115	185	40.05	51.1	55.3	57.9	60.1	8.7	9.1	11.1	12.1	13.2	53.65	41.7	30.2	31.3	20	1530	2
M-Z	4	355	115	185	40.95	52.7	56.8	58.1	60.8	8.8	9.3	11.2	12.3	13.3	53.8	41.8	30.2	31.4	20	1530	2
M-B	4	350	120	190	39.12	49.5	54.2	55.4	58.7	8.6	9.1	10.9	11.8	13.1	53.2	41.2	30.1	31.3	19	1520	2
M-Pr	1	275	175	250	23.1	29.2	32.4	37.9	39.6	5.1	5.4	5.9	6.4	7.1	36.1	35.2	32.8	32.6	26	1580	1
M-V	1	275	175	245	27.3	33.2	38.6	41.2	44.1	5.2	5.7	6.3	6.7	7.3	40.2	35.1	33.4	33.2	16	1460	1
M-Py	3	325	165	230	31.4	41.5	46.9	48.9	50.5	6.7	7.4	8.5	9.3	9.5	48.5	43.2	40	40.2	26	1580	2
M-MS	4	360	110	160	45.5	56.9	61.2	64.2	65.1	8.8	9.1	9.9	10.5	11.3	57.8	49.2	38.9	39	20	1530	2
M-SF	4	355	115	170	45.3	56.4	60.7	62.3	62.5	8.7	9	9.7	10.3	11.2	56.8	47.8	36.1	36	20	1530	2
M-Sp	2	375	90	155	57.8	73.1	78.2	84.5	90.1	9.5	12	14.8	16.5	17.8	88.6	80.1	63.7	50.3	34	1750	3
M-CG	3	370	90	155	53.9	68.9	76.2	82	85.1	9.3	11.8	14.5	16.3	16.8	82.5	73.5	64.2	47.3	19	1520	2
M-Cc	3	370	90	155	54.1	69.1	76.9	82.5	85.8	9.3	11.9	14.6	16.5	17	85.5	80.2	64.8	49.9	27	1610	2
M-Kc	3	350	125	200	37.2	47.7	50.8	53.1	57.8	7.8	8.3	10.2	10.9	11.7	54.8	43.8	35.2	33.4	30	1670	2
M-Ap	3	375	90	155	62.1	78.9	84.2	88.5	93.2	9.7	12.3	14.9	17	18.6	88.9	85.1	64.2	50.1	38	1850	3
M-L	4	370	105	160	46.5	59.3	61.2	62.3	62.5	8.8	9.3	9.4	9.5	9.5	35.2	17.5	13.1	12.8	7	1230	1
M-T	1	270	100	300	48	49.3	53.6	65.2	71.3	8.2	8.2	8.5	9.4	12.9	67.5	62.3	55.2	53.2	13	1380	2
M-CS	3	300	180	255	23.5	35.1	49.2	55.5	63.8	5.1	5.5	6.3	10.5	11.8	55	20.6	17.1	16.5	9	1200	2

3.2. Cluster analyses of experimental mortars

A dendrogram of experimental mortars using complete linkage as an amalgamation rule and the city block (Manhattan) distance as a measure of the nearness among samples is illustrated in Fig. 2.

The dendrogram built on the experimental data explained appropriate distinctiveness between samples. There are three clusters of samples. As presented in Fig. 2, there is high resemblance between M-OPC, M-HSCR, M-MHHC, M-HESC, and M-LHHC mortars. Only mortars based on masonry cements are in this cluster. This group of samples that shapes the first cluster is described by the most notable IST and FST values, as well as high early and final compressive (CCS-3, CCS-7, CCS-14, CCS-21, CCS-28) and flexural strengths (CFS-3, CFS-7, CFS-14, CFS-21, CFS-28). Altered mortars with addition of copper slag, limestone, and talc (M-CS, M-L, M-T) are conjoined in this cluster due to the similarity in the observed outputs (high IST, FST, CCS, and CFS).

The second cluster associated the following altered mortars: M-FA, M-MS, M-SF, M-BA, M-Z, M-B, M-Py, M-Kc, M-Pr, and M-V. The class of mortar samples that pertains to the second cluster exhibited values of variables that were slightly below values displayed for cement mortars from the first cluster. This was expected because mineral raw materials employed in the design of mortars as a cement replacement tend to deteriorate performances of mortar at least to a certain extent. However, here it was showed (Table. III, Fig. 2) that the application of economical primary and/or secondary mineral additives such as fly ash, bottom ash, zeolite, bentonite, perlite, vermiculite, pyrophyllite, micro silica, silica fume, and kaolin clay induce comparatively good physico-mechanical and thermo-mechanical properties of mortars. Namely, this cluster is directly connected to first cluster indicating strong similarities between standard cement mortars and altered mortars based on additives of primary and secondary origin. The given group of mortars is depicted by high compressive and flexural strengths, with accent on towering late CCS-28 and FCS-28 strengths. Even though altered mortars from cluster two are classified as masonry mortars, they also exhibit excellent thermal properties such as high refractoriness and relatively high hot compressive strengths (which grouped them together in cluster two and distinguished them from standard masonry mortars from cluster one).

The remaining mortar samples (M-CAC, M-HAC, M-CG, M-Cc, M-Sp, and M-Ap) represent the third cluster since all of the samples are depicted by high values of HH, SR, SK-T, SK, HCS-100, HCS-500, HCS-800, and HCS-1000. The cement mortars that also belong to this group i.e., cluster three, are high-temperature resistant mortars based on calcium-aluminate and high-aluminate cement (M-CAC and M-HAC). Mineral additives such as spinel, chamotte, calcinated clay, and alumina can be considered as appropriate for high-temperature applications since they induced high hot compressive strengths in observed mortar samples.

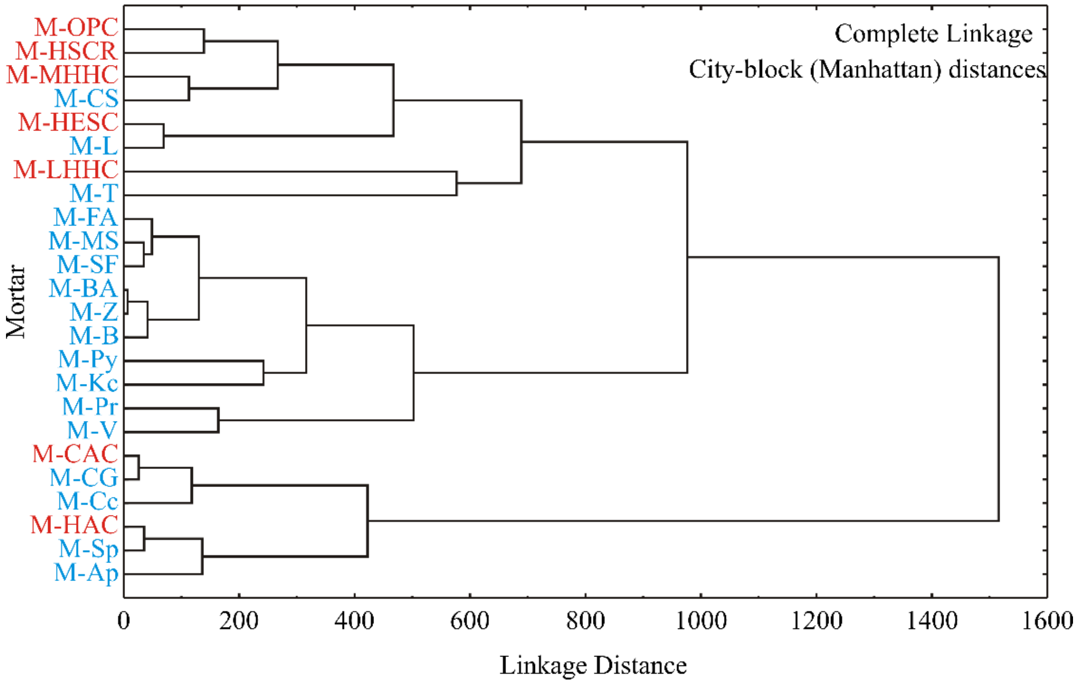

Fig. 2. Complete-linkage dendrogram of cement mortars and altered mortars.

3.3. Principal component analysis (PCA) of outputs

The PCA permitted an extensive depletion in a number of variables and the uncovering of structure in the association between measured parameters and chosen outputs (Fig. 3). As can be seen, there is a clean segregation of the 24 trials. Quality outcomes show that the first two principal components, accounting for 81.78 % of the total variability can be considered sufficient for data representation. Variables CCS-3, CCS-7, CCS-14, CCS-21, CCS-28, CFS-3, CFS-7, CFS-14, CFS-21, CFS-28, and HCS-100, HCS-500, HCS-800, HCS-1000 supplied the most negatively to the first principal component estimation (4.2-6.3 % of total variance, based on correlation). The most positive impact to the second principal component was identified for PA (22.2 %) and HH (8.2 %), while the most negative effect to the second principal component was esteemed for HCS-500, HCS-800 and HCS-1000 (5.6, 8.4 and 12.6 %, accordingly) and FST (5.1 %).

The effects of processing parameters are illustrated in Fig. 3, with higher IST and FST values at the right side of graphic, while the more HH, SR, SK, SK-t, CCS-7, CCS-14, CCS-21, CCS-28; CFS-3, CFS-7, CFS-14, CFS-21, CFS-28, HCS-100, HCS-500, HCS-800, and HCS-1000 values are discovered at the left side of graphic. This is in agreement with Cluster Analysis. Namely, M-OPC, M-HSCR, M-MHHC, M-HESC, M-LHHC, M-CS, M-L, and M-T located on the right side of the graph showed the highest IST and FST values (also situated on the right side of PCA biplot). M-T sample is set somewhat apart from this group because it showed slight difference in the observed characteristics i.e., higher value of final setting time. M-FA, M-MS, M-SF, M-BA, M-Z, M-B, M-Py, M-Kc, M-Pr, and M-V samples are grouped around center of the diagram exhibiting good compressive and flexural strengths. Finally, M-CAC, M-HAC, M-CG, M-Cc, M-Sp, and M-Ap are on the left side of the graph where the highest cold and hot mechanical strengths are placed. These mortars belong to group of thermally resistant materials.

PCA graphic explained over-all good discernment attitude between all trials, which were discovered distinct due to variants in output variables measured in samples.

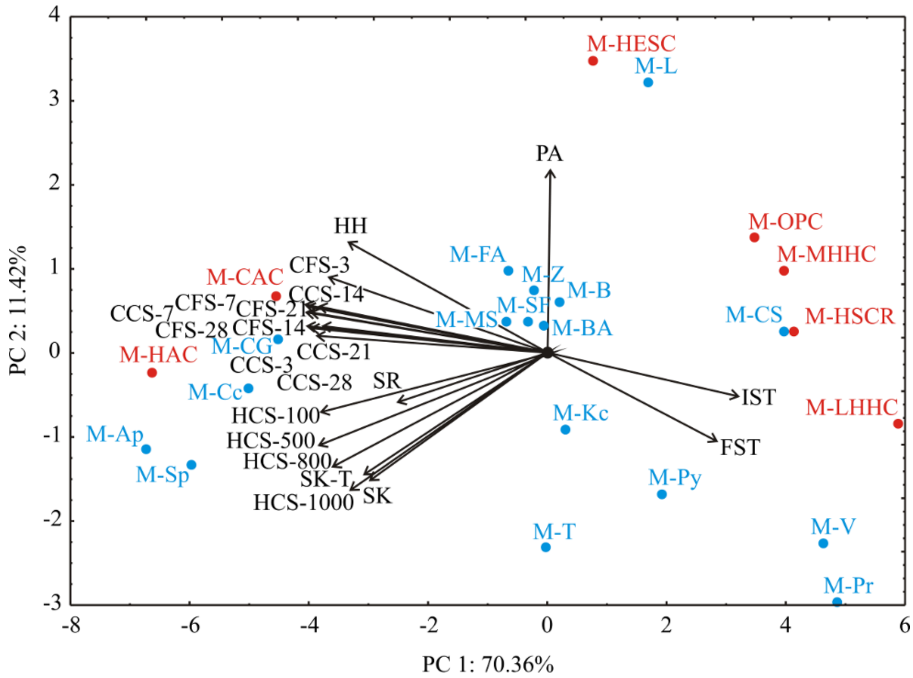

Fig. 3. Biplot for mechanical characteristics of cement mortars and altered mortars.

3.4. Neurons in the ANN hidden layer

Broyden–Fletcher–Goldfarb–Shanno (BFGS) algorithm, conducted in StatSoft Statistica's evaluation routine, was used for ANN modeling. The optimum number of hidden neurons was selected in order to minimize the distinction among expected ANN values and intended outputs. SOS was applied throughout testing as accomplishment indicator. In line with ANN performance (sum of r^2 and SOSs for all variables in one ANN), it was seen that the optimal number of neurons in the hidden layer is 13 (network MLP 10-13-21), when obtaining high values of r^2 (0.999; 0.998 and 0.999 for training, testing and validation performances, respectively) and also low values of SOS (Table IV).

Tab. IV ANN summary (performance and errors), for training, testing and validation cycles.

Network name	Performance			Error		
	Training	Test	Validation	Training	Test	Validation
MLP 10-13-21	0.999	0.998	0.999	15.171	16.254	15.925
	Training algorithm	Error function		Hidden activation		Output activation
	BFGS 724	SOS		Logistic		Exponential

*Performance term represent the coefficients of determination, while error terms indicate a lack of data for the ANN model.

The ANN model is complex (437 weights-biases) according to the high nonlinearity of the developed system [42]. The r^2 values between experimental measurements and ANN model outputs, PA, HH, IST, FST, CCS-3, CCS-7, CCS-14, CCS-21, CCS-28, CFS-3, CFS-7, CFS-14, CFS-21, CFS-28, HCS-100, HCS-500, HCS-800, HCS-1000, SK, SK-T, and SR were between 0.999 and 1.000, during the training period.

Table V presents the elements of matrix W_1 and vector B_1 (presented in the bias row), and Table VI presents the elements of matrix W_2 and vector B_2 (bias) for the hidden layer.

Tab. V Elements of matrix W_1 and vector B_1 (presented in the bias row).

	1	2	3	4	5	6	7	8	9	10	11	12	13
SiO_2	-5.773	24.537	-4.817	-17.630	-5.157	1.446	24.942	33.087	46.500	-18.701	-6.117	-3.169	9.364
Al_2O_3	-36.026	-3.678	-44.286	-25.270	-47.336	-50.056	-47.296	24.828	-45.254	-46.460	-36.108	-49.299	-39.618
Fe_2O_3	8.081	-34.571	-5.593	-8.966	32.391	11.297	15.435	21.461	-28.841	-10.952	9.197	39.762	6.548
CaO	51.404	8.092	20.413	20.807	20.184	23.276	30.123	34.755	34.386	40.260	81.709	36.625	29.221
MgO	-11.381	-30.164	28.248	-40.618	-22.348	19.330	-27.738	1.004	27.460	-5.031	15.726	-13.161	-22.644
K_2O	27.161	-50.482	8.892	58.693	58.131	46.657	44.097	44.902	37.098	49.003	31.672	18.671	-13.208
Na_2O	-21.998	3.545	-1.200	7.409	3.199	-2.838	7.452	3.363	-1.004	1.889	23.565	0.474	-17.092
TiO_2	-9.410	3.259	-5.069	11.798	-13.554	-56.399	-33.918	-9.967	8.383	1.835	-21.072	-13.392	-57.132
SO_3	24.166	12.892	2.166	-0.507	-9.584	-15.963	-4.513	-7.348	-23.750	-1.554	-68.467	-3.980	-4.545
LoI	-25.021	-33.207	-22.448	43.478	-15.713	-1.628	-3.358	0.767	-44.252	17.362	-60.493	23.023	2.266
Bias	-7.967	-3.515	3.977	-24.081	-0.966	-21.491	-8.036	-39.231	-20.873	-31.606	-15.233	3.201	-24.058

The quality of the model fit was investigated and the residual analysis of the established model was exposed in Table VII.

The ANN model had a negligible lack of fit tests, which means the model satisfactorily predicted the quality of cements and additives. A high r^2 is illustrative that the variation was constituent for and that the data fitted the proposed model effectively.

Tab. VI Elements of matrix W_2 and vector B_2 (presented in the bias column).

	1	2	3	4	5	6	7	8	9	10	11	12	13	Bias
PA	-16.278	30.841	-91.579	-26.836	34.290	-39.050	-2.625	2.837	-1.435	13.485	43.447	-6.391	62.178	-0.718
HH	7.642	1.328	-6.256	5.184	1.218	0.422	-0.278	10.393	4.280	0.563	-13.942	-5.958	-7.818	0.015
IST	26.278	-10.519	-9.314	1.637	-3.275	9.398	22.297	4.859	12.477	-3.210	-8.643	-26.761	-17.309	-5.385
FST	16.086	-21.088	10.339	-6.920	-18.984	7.324	44.644	-9.510	1.380	0.951	14.475	-28.205	-19.586	-11.890
CCS-3	8.496	2.477	-12.742	-11.334	6.445	19.436	-1.658	12.162	8.201	3.720	-19.581	-9.451	13.040	0.003
CCS-7	-2.316	3.027	-13.497	-31.707	16.392	33.947	-2.457	-8.960	4.307	12.207	-7.321	-3.008	30.616	-0.002
CCS-14	7.921	1.669	-10.723	-4.697	8.342	9.182	-2.202	8.123	8.349	0.385	-14.895	-8.494	7.872	-0.008
CCS-21	7.719	1.231	-10.197	-0.980	13.039	2.045	-3.367	4.002	9.832	-1.060	-14.152	-8.756	4.977	0.004
CCS-28	6.725	1.061	-10.107	-3.537	12.992	3.356	-2.894	3.636	9.512	-1.056	-12.573	-8.917	8.864	0.003
CFS-3	20.003	2.409	-3.139	25.217	-21.643	-11.100	-0.187	51.599	6.867	-11.555	-33.185	-12.761	-16.886	-0.027
CFS-7	20.821	2.658	-4.677	25.182	-20.467	-10.897	-1.305	51.749	7.938	-11.722	-33.829	-13.033	-16.336	-0.031
CFS-14	20.445	2.638	-3.253	28.772	-23.463	-15.806	-1.402	55.909	7.320	-12.099	-35.106	-12.875	-19.675	-0.038
CFS-21	0.450	1.608	-4.337	-5.257	4.224	0.088	-3.086	6.178	3.286	-0.219	-6.455	-2.558	11.470	-0.014
CFS-28	1.783	0.964	-7.136	-8.844	10.049	1.841	-2.635	3.862	6.527	0.262	-8.669	-6.133	15.713	-0.011
HCS-100	-18.706	2.696	-3.958	-36.258	14.714	18.243	-4.902	-18.972	-1.836	8.384	17.088	6.180	-42.329	-0.041
HCS-500	-1.439	0.121	-6.061	-1.955	9.259	-0.942	-2.781	-2.315	6.303	1.168	-1.539	-4.302	-3.829	-0.022
HCS-800	-8.939	1.117	-1.934	-12.440	6.951	6.482	-3.896	-11.499	-0.324	4.243	8.917	4.259	-28.322	-0.021
HCS-1000	-22.429	1.946	-0.663	-33.039	8.306	16.169	-3.848	-18.843	-4.269	8.603	22.935	8.840	-40.507	-0.117
SK	10.854	-6.497	-23.241	6.876	27.272	-9.957	4.235	-3.793	26.802	0.881	-9.604	-29.223	-12.888	0.019
SK-T	15.922	-5.234	-21.741	8.370	24.507	-5.566	3.699	-0.870	24.324	-0.982	-15.112	-26.886	-7.272	-0.007
SR	34.723	-2.247	-0.880	-66.442	-27.336	-54.253	0.778	66.151	16.327	-45.476	-32.347	-22.889	71.610	0.005

Tab. VII The "goodness of fit" tests for the developed ANN model.

	χ^2	RMSE	MBE	MPE	r^2	Residual analysis			
						Skewness	Kurtosis	Average	SD
PA	0.000	0.002	0.000	0.047	1.000	-1.271	3.054	0.000	0.002
HH	12.213	1.427	-0.007	0.312	0.999	0.845	1.979	-0.005	1.262
IST	0.697	0.341	-0.098	0.248	1.000	1.307	2.911	-0.074	0.292
FST	16.437	1.655	0.038	0.503	1.000	-0.485	5.355	0.028	1.464
CCS-3	0.610	0.319	-0.012	0.679	1.000	1.550	5.078	-0.009	0.282
CCS-7	0.236	0.198	-0.010	0.373	1.000	0.353	1.703	-0.008	0.175
CCS-14	1.586	0.514	-0.008	0.725	0.999	-0.993	1.396	-0.006	0.455
CCS-21	0.877	0.382	-0.026	0.565	1.000	0.137	0.176	-0.019	0.338
CCS-28	1.199	0.447	-0.013	0.622	0.999	-0.274	0.865	-0.010	0.395
CFS-3	0.006	0.031	0.000	0.350	1.000	-0.355	0.011	0.000	0.027
CFS-7	0.011	0.043	0.001	0.406	1.000	-0.374	1.837	0.001	0.038
CFS-14	0.022	0.061	-0.005	0.550	1.000	0.622	0.711	-0.004	0.054
CFS-21	0.020	0.058	-0.002	0.324	1.000	-0.619	2.317	-0.001	0.051
CFS-28	0.068	0.106	0.003	0.536	0.999	0.645	2.316	0.002	0.094
HCS-100	2.830	0.687	-0.014	0.932	0.999	-0.348	2.692	-0.011	0.607
HCS-500	3.481	0.762	0.028	1.280	0.999	-0.164	1.263	0.021	0.673
HCS-800	0.541	0.300	-0.008	0.666	1.000	0.214	1.762	-0.006	0.266
HCS-1k	2.605	0.659	0.067	1.620	0.998	1.816	4.383	0.051	0.581
SK	1.691	0.531	0.104	2.251	0.998	3.087	13.067	0.078	0.463
SK-T	197.611	5.739	-0.169	0.268	0.999	-0.385	2.402	-0.127	5.075
SR	0.000	0.004	0.000	0.138	1.000	-0.252	2.407	0.000	0.004

The mean and the standard deviation of residuals have also been analyzed. The mean of residuals for ANN model for PA, HH, IST, FST, CCS-3, CCS-7, CCS-14, CCS-21, CCS-28, CFS-3, CFS-7, CFS-14, CFS-21, CFS-28, HCS-100, HCS-500, HCS-800, HCS-1000, SK, SK-T, and SR prediction were: 0.000; -0.005; -0.074; 0.028; -0.009; -0.008; -0.006; -0.019; -0.010; 0.000; 0.001; -0.004; -0.001; 0.002; -0.011; 0.021; -0.006; 0.051; 0.078; -0.127 and 0.000, respectively, while the standard deviations were: 0.002; 1.262; 0.292; 1.464; 0.282; 0.175; 0.455; 0.338; 0.395; 0.027; 0.038; 0.054; 0.051; 0.094; 0.607; 0.673; 0.266; 0.581; 0.463; 5.075 and 0.004. These results revealed a good estimation to a normal distribution around zero with a probability of 95% (2•SD), which means a good generalization ability of ANN model for the range of observed experimental values.

3.5. Sensitivity analysis

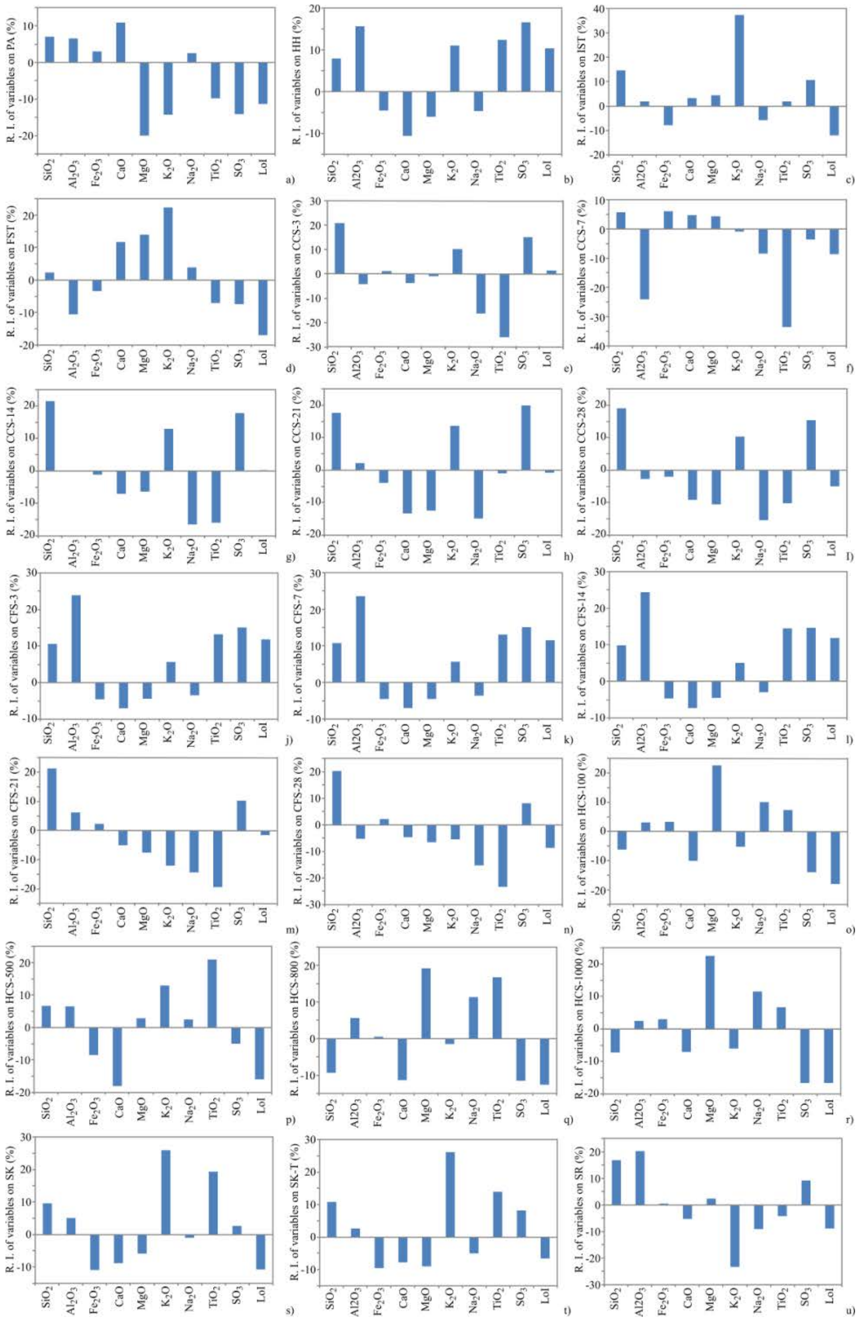

Fig. 4. Relative influence in outputs (mortar properties) according to changes in input variables (chemical composition).

In order to entry the impacts of variations in the outputs in line with the variations in the inputs, a sensitivity analysis was accomplished. The greater effect recorded in the output means more augmented sensitivity in respect to the input. The effects of the input factors over the outputs are expressed in Fig. 4, by evaluated changes in outputs, for infinitesimal changes in inputs. Acquired values corresponded to degree of experimental errors, and also showed the inputs influence on outputs.

As it is illustrated in Fig. 4., PA parameter was mostly influenced by CaO. The changes in the contents of Al_2O_3 and SiO_2 performed lesser effect on the pozzolanic activity of a mineral additive. Presence of magnesium and potassium negatively influenced PA.

The heat of hydration (HH) was most significantly influenced by Al_2O_3 content. Calcium oxide detected in the observed mineral additives had negative effect on HH. Initial setting times (IST) were mostly influenced by K_2O i.e., altered mortars with most significant variations in potassium content. Variations in final setting times (FST) were determined through changes in greater number of oxides: K_2O, Al_2O_3, CaO, and MgO.

Variations registered for compressive strengths (CCS) showed interesting route over twenty-eight days period. CCS-3 was strongly influenced by SiO_2 content (R.I. = 20 %). CCS-7 was negatively influenced by Al_2O_3 content (R.I = -25%). CCS-14, CCS-21, and CSS-28 were equally influenced by SiO_2 (R.I. = 20%), while R.I. of calcium and magnesium oxides varied from 7 % to 15 % to 10 %, respectively.

Sensitivity analysis diagrams showed no significant difference for flexural strengths up to 14th day of testing. CFS-3, CFS-7, and CFS-14 were mostly influenced by Al_2O_3 (R.I. being approximately 25 %), followed by SiO_2 (R.I. = 10 %). CFS-21 and CFS-28 were mostly influenced by alternations in SiO_2 content (R.I. = 20 %).

Hot compressive strength measured upon firing at 100°C was strongly influenced by variation of MgO content (R.I. = 22 %). Variations in LoI had the strongest negative influence on this parameter (R.I. = -18 %). Variations in CaO (R.I. = -18 %), TiO_2 (R.I. = 19%) and LoI (R.I. = -10 %) exhibited the strongest influence over HCS-500 strength. HCS-800 was determined by variations in SiO_2 (R.I. = -10 %), Al_2O_3 (R.I = 5 %), CaO (R.I. = -12 %), MgO (R. I. = 19 %), TiO_2 (R.I. = 17 %), and LoI (R.I = 13 %). HCS-1000 was similarly influenced by variations of the same oxides: SiO_2 (R.I. = -7 %), Al_2O_3 (R.I = 3 %), CaO (R.I. = -6 %), MgO (R. I. = 21 %), TiO_2 (R.I. = 17 %), and LoI (R.I = 17 %).

Variations of Fe_2O_3 and K_2O performed the strongest influence over refractoriness. Sulphate resistance of observed mortar samples was affected by variations in SiO_2, Al_2O_3, K_2O, SO_3 and LoI contents.

4. Conclusion

Analytical analyses and Artificial neural network (ANN) modeling were employed to foresee the quality of mortars designed on given seven types of cement and seventeen mineral additives. The impacts that chemical compositions of implemented raw materials are making on the quality (properties) of the designed mortars were assessed and evaluated.

The CA dendrogram built on the experimental data and PCA biplot explained appropriate distinctiveness between samples by creating three groups of mortars. The first group associated mortars based on masonry cements due to high early and final compressive and flexural strengths. Altered mortars with addition of copper slag, limestone, and talc were conjoined in this cluster due to the similarity in setting times. The second group distinguished and separated altered mortars (M-FA, M-MS, M-SF, M-BA, M-Z, M-B, M-Py, M-Kc, M-Pr, and M-V). The second cluster was directly connected to first cluster indicating strong similarities between standard cement mortars and altered mortars based on mineral additives of primary and secondary origin. The given group of mortars is depicted by high compressive and flexural strengths, but also excellent thermal properties (refractoriness and hot compressive strength). The remaining mortar samples (mortars based on calcium-aluminate and high-aluminate cement, and mortars altered by addition of spinel, chamotte, calcinated clay, and alumina) represent the third cluster which is depicted by high values of hot compressive strength, refractories, and sulphate resistance.

Impacts of variations in the outputs in line with the variations in the inputs were determined via sensitivity analysis. Variations in CaO conveyed the greatest influence on pozzolanic activity. The heat of hydration was influenced by Al_2O_3 content. Setting times were mostly influenced by K_2O. Early and final compressive strengths were positively influenced by SiO_2. Only compressive strength measured after seven days was negatively influenced by Al_2O_3 content. Early flexural strengths were influenced by Al_2O_3, while final strengths were mostly influenced by alternations in SiO_2 content. Hot compressive strength (100°C) was influenced by variation of MgO content. Compressive strength (1000°C) was additionally influenced by variations in the SiO_2, Al_2O_3, CaO, and TiO_2. Variations of Fe_2O_3 and K_2O performed the strongest influence over refractoriness. Sulphate resistance of observed mortar samples was affected by variations in SiO_2, Al_2O_3, K_2O, SO_3 and LoI contents.

The obtained ANN outputs highlight the high suitability level of anticipation, i.e., 0.999 during the training period, which can be regarded appropriately enough to correctly predict the observed outputs in a wide range of experimental parameters. The developed ANN model displays high predictive accuracy and can replace or be used in combination with standard destructive tests thereby saving the construction industry time, resources, and capital.

Acknowledgments

This investigation is financially supported by Ministry of Education, Science and Technological Development of the Republic of Serbia (contract no.: 451-03-68/2022-14/ 200012)

5. References

1. M. Azimi-Pour, H. Eskandari-Naddaf, Constr. Build. Mater. 189 (2018) 978.
2. Z. Zhang, B. Zhang, P. Yan, Constr. Build. Mater. 105 (2016) 82.
3. H. Eskandari, A.M. Nic, A. Ghanei, Procedia Eng. 150 (2016) 2178.
4. Madadi, H. Eskandari-Naddaf, M. Gharouni-Nik, Arab. J. Sci. Eng. (2017) 1.
5. E. Bernal, M. Vlasova, P. Márquez, M. Kakazeyl, R. Tapia, Sci. Sint. 52 (2020) 25.
6. L.G. Li, J. Zhu, Z.H. Huang, A.K.H. Kwan, L.J. Li, Constr. Build. Mater. 157 (2017) 337.
7. Z. Bajja et al., Constr. Build. Mater. 132 (2017) 85.
8. M. Rostami, K. Behfarnia, Constr. Build. Mater. 134 (2017) 262-268.
9. Terzić, M. Dojčinović, Lj. Miličić, J. Stojanović, Z. Radojević, Sci. Sint. 53 (2021) 445.
10. H. Li et al., Compos. B Eng. 35 (2) (2004) 185.
11. S. Ozen, B. Liguori, B. De Gennaro, P. Cappelletti, G.D. Gatta, F. Iucolano, C. Colella, Constr. Build. Mater. 105 (2016) 46.
12. G. Mertens, R. Snellings, K. Van Balen, B. Bicer-Simsir, P. Verlooy, J. Elsen, Cem. Concr. Res. 39 (2009) 233.
13. Faheem, S. Ali Rizwan, T. Bier, Constr. Build. Mater. 286 (2021) 122788.
14. Purbasari, D. Ariyanti, S. Sumardiono, M. Anif Shofa, R. Parasian Manullang, Sci. Sint. 54 (2022) 45.
15. F.A. Sabet, N.A. Libre, M. Shekarchi, Constr. Build. Mater. 44 (2013) 175.

16. T.B.T. Nguyen, R. Chatchawan, W. Saengsoy, S. Tangtermsirikul, T. Sugiyama, Constr. Build. Mater. 209 (2019) 176.
17. P.R. de Matos, M. Foiato, L.R. Prudêncio, Constr. Build. Mater. 203 (2019) 282.
18. S. Ahmad, S.A. Barbhuiya, A. Elahi, J. Iqbal, Clay Miner. 46 (1) (2018) 85.
19. L. Mengliang, H. Yang, L. Zhenyu, Y. Tao, H. Xin, W. Jie, L. Zhongyuan, L. Shuzhen, Constr. Build. Mater. 241 (2020) 118015.
20. Q. Ma, H. Du, X. Zhou, K. He, Z. Lin, F. Yan, L. Huang, R. Guo, Constr. Build. Mater. 172 (2018) 378.
21. A.K. Parande, B. Ramesh Babu, M. Aswin Karthik, K.K. Deepak Kumaar, N. Palaniswamy, Constr. Build. Mater. 22 (3) (2008) 127.
22. R. Kaminskas, R. Kubiliute, B. Prialgauskaite, Cem. Concr. Compos. 113 (2020) 103710
23. I. Bozyigit, F. Bulbul, C. Alp, S. Altun, Eng. Sci. Technol. 24 (5) (2021) 090.
24. Q. Shao, K. Zheng, X. Zhou, J. Zhou, X. Zeng, Cem. Concr. Compos. 98 (2019) 39.
25. S. Celikten, M. Sarıdemir, K.y Akçaozoglu, J. Build. Eng. 32 (2020) 101717.
26. M. Karatas, A. Benli, H.Anil Toprak, Constr. Build. Mater. 221 (2019) 163–176.
27. G. Wu, W. Yan, S. Schafföner, X. Lin, S. Ma, Y. Zhai, X. Liu, Lin. Xu, Constr. Build. Mater. 185 (2018) 102.
28. K. Shiota, T. Nakamura, M. Takaoka, et al., J. Environ. Manag. 201 (2017) 327.
29. M. Sarıdemir, Mater. Des. 56 (2014) 297.
30. H. Eskandari-Naddaf, R. Kazemi, Constr. Build. Mater. 138 (2017) 1.
31. F. Özcan, Constr. Build. Mater. 26 (1) (2012) 404-410.
32. S. Chithra et al., Constr. Build. Mater.114 (2016) 528.
33. F. Özcan et al., Adv.Eng. Softw. 40 (9) (2009) 856.
34. M. Sarıdemir, Adv. Eng. Softw. 40 (5) (2009) 350.
35. A. Terzić, L. Pezo, Lj. Andrić, Sic. Sint. 49 (4) (2017) 381.
36. H. Abdi, L. Williams, Principal component analysis, Wiley Interdisciplinary Reviews. Comp. Stat. 2 (2010) 433.
37. B.J. Taylor, Methods and Procedures for the Verification and Validation of Artificial Neural Networks, Springer, US, 2006.
38. A. Terzić, D. Radulović, M. Pezo, J. Stojanović, L. Pezo, Z. Radojević, Lj. Andrić, Constr. Build. Mater. 258 (2020) 119721.
39. T. Kollo, D. von Rosen, Advanced Multivariate Statistics with Matrices, Springer, Netherlands, 2005.
40. G. H. Yoon, A. Donoso, J. Bellido, D. Ruiz, Int. J. Numer. Met. Eng. 121 (20) (2020) 4473.

Сажетак: *Предвиђање перформанси грађевинских материјала а тиме и оптимизација њихових састава коришћењем модела за машинско учења је есенцијални део савременог грађевинарства. У овом раду је спроведена прогноза понашања малтера заснована на примени модела вештачких неуронских мрежа (АНН). Добијени модел се употребљава за процену дизајна и карактеристика седамнаест грађевинских или високо-температурних малтера. Примењено је седам врста цемента. Седамнаест минералних адитива примарног и секундарног порекла употребљене су у малтерним мешавинама. Анализа кластера и анализа главних компоненти означиле су групе сличних малтера чији су састав и својства измењени употребом минералних адитива и груписале их према специфичности намене на основу разматраних карактеристика. Модел вештачких неуронских мрежа је коришћен за предвиђање квалитета малтера. Процењени су и прогнозирани утицаји које хемијски састав сировина има на квалитет малтера. Добијени АНН излази имају висок ниво антиципације - 0,999 током периода обуке, што се може сматрати задовољавајуће за прецизно предвиђање резултата у*

широком опсегу процесних параметара. Развијени АНН модел показује високу тачност предвиђања и може да замени или да се користи у комбинацији са стандардним деструктивним тестовима чиме се штеди време, ресурси и капитал у грађевинској индустрији. Добре перформансе експерименталних цементних малтера су позитиван знак у смислу ширења праксе примене економичних минералних адитива у грађевинским материјалима и постизања смањења емисије угљен диоксида.
***Кључне речи**: Грађевински цементи; високо-температурни цементи; индустријски нуспроизводи; економичне примарне сировине; циркуларна економија.*